

Bi-level Feature Alignment for Versatile Image Translation and Manipulation

Fangneng Zhan*, Yingchen Yu*, Rongliang Wu, Kaiwen Cui, Aoran Xiao,
Shijian Lu[§], Ling Shao, Fellow, IEEE

Abstract—Generative adversarial networks (GANs) have achieved great success in image translation and manipulation. However, high-fidelity image generation with faithful style control remains a grand challenge in computer vision. This paper presents a versatile image translation and manipulation framework that achieves accurate semantic and style guidance in image generation by explicitly building a correspondence. To handle the quadratic complexity incurred by building the dense correspondences, we introduce a bi-level feature alignment strategy that adopts a top- k operation to rank block-wise features followed by dense attention between block features which reduces memory cost substantially. As the top- k operation involves index swapping which precludes the gradient propagation, we propose to approximate the non-differentiable top- k operation with a regularized earth mover’s problem so that its gradient can be effectively back-propagated. In addition, we design a novel semantic position encoding mechanism that builds up coordinate for each individual semantic region to preserve texture structures while building correspondences. Further, we design a novel confidence feature injection module which mitigates mismatch problem by fusing features adaptively according to the reliability of built correspondences. Extensive experiments show that our method achieves superior performance qualitatively and quantitatively as compared with the state-of-the-art. The code is available at <https://github.com/fnzhan/RABIT>.

Index Terms—Image Translation, Image Manipulation, Image Correspondence, Generative Adversarial Networks.

1 INTRODUCTION

IMAGE translation and manipulation aim to generate and edit photo-realistic images conditioning on certain inputs such as semantic segmentation [54], [65], key points [11], [60] and layout [35]. It has been studied intensively in recent years thanks to its wide spectrum of applications in various tasks [51], [56], [63]. However, achieving high fidelity image translation and manipulation with faithful style control remains a grand challenge due to the high complexity of natural image styles. A typical approach to control image styles is to encode image features into a latent space with certain regularization (e.g., Gaussian distribution) on the latent feature distribution. For example, Park *et al.* [54] utilize VAE [10] to regularize the distribution of encoded features for faithful style control. However, VAE struggles to encode the complex distribution of natural image styles and often suffers from *posterior collapse* [45] which leads to degraded style control performance. Another strategy is to encode reference images into style codes to provide style guidance in image generation. Choi *et al.* [5] employ a style encoder to extract the style code from a given reference image and achieve diverse image synthesis over multiple domains. Zhu *et al.* [95] further propose to extract style codes for each semantic region individually and achieve flexible style control within each semantic region. However, style codes often capture the overall image style or local region style without an explicit style guidance in spatial domain.

Recently, building dense correspondences between images has attracted increasing interest in image translation and manipulation

thanks to its impressive image generation performance. Prior studies have explored to build correspondences between images of the same domain for exemplar-based image colorization [17], [85]. Zhang *et al.* [87] further explore to build cross-domain correspondences with Cosine similarity to achieve exemplar-based image translation. However, Zhang *et al.* construct the semantic correspondences based on Cosine similarity that often leads to many-to-one matching (i.e. multiple conditional input features match to the same exemplar feature). Zhan *et al.* [78] thus propose to build the correspondence with optimal transport which facilitates the mass preserving property to mitigate the many-to-one matching. On the other hand, building dense correspondences has quadratic complexity which incurs high memory costs and struggles while scaling up to high-resolution images. To achieve high-resolution image translation, Zhou *et al.* [93] propose a GRU-assisted Patch-Match [1] method to build high-resolution correspondences efficiently. Zheng *et al.* [90] tackle the high-resolution correspondences via sparse attention with applications to semantic image manipulation. However, all above methods aim to build correspondences based on their semantic coherence without consideration of their structure coherence. As textures within a semantic region share identical semantic information, the texture structure information tends to be lost while building pure semantic correspondence. Warping exemplars with such pure semantic correspondence will further cause destroyed texture patterns in the warped exemplars which provide inaccurate guidance for image generation.

This paper presents **RABIT**, a **R**anking and **A**ttention scheme with **B**i-level feature alignment for versatile **I**mage **T**ranslation and manipulation. RABIT consists of an alignment network and a generation network that are optimized jointly. The alignment network establishes feature correspondences between a conditional input (semantic guidance) and an exemplar (style guidance). With

• F. Zhan, Y. Yu, R. Wu, K. Cui, A. Xiao, and S. Lu are with the School of Computer Science and Engineering, Nanyang Technological University, Singapore, 639798. L. Shao is with the Inception Institute of Artificial Intelligence, UAE, 111999.

* denotes equal contribution. [§] denotes corresponding author, E-mail: shijian.lu@ntu.edu.sg.

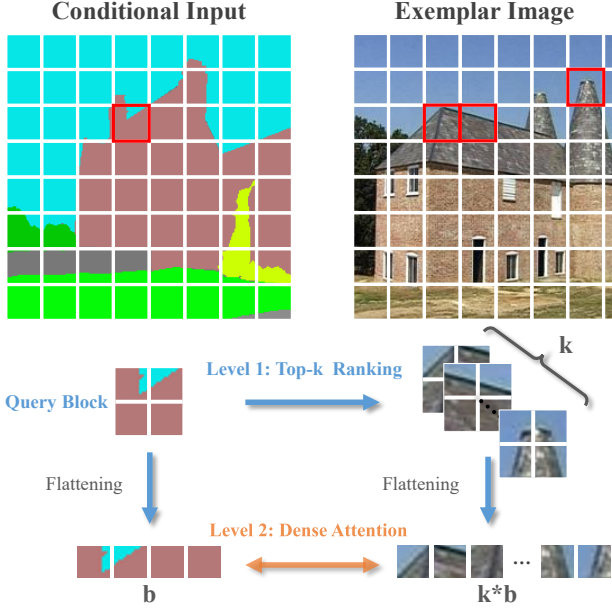


Fig. 1. Bi-level feature alignment via ranking and attention scheme: With a query block from the *Conditional Input*, we first retrieve the top- k most similar blocks from the *Exemplar Image* through a differentiable ranking operation, and then compute dense attention between features in query block and features in retrieved top- k blocks. Such bi-level alignment reduces the computational cost greatly, and it also allows to build high-resolution correspondences which leads to more realistic translation with finer details.

the built correspondences, the exemplar is warped to be aligned with the conditional input to provide accurate style guidance for the generation network. However, building dense correspondence incurs quadratic computational complexity which struggles with high-resolution correspondences. We design a bi-level alignment strategy with a Ranking and Attention Scheme (RAS) which builds feature correspondences efficiently at two levels: 1) a top- k ranking operation for dynamically generating block-wise ranking matrices; 2) a dense attention module that achieves dense correspondences between features within blocks as illustrated in Fig. 1. RAS enables to build high-resolution correspondences and reduces the memory cost from $\mathcal{O}(L^2)$ to $\mathcal{O}(N^2 + b^2)$ (L is the number of features for alignment, b is block size, and $N = \frac{L}{b}$). However, the top- k operation involves index swapping whose gradient cannot be propagated in networks. To address this issue, we approximate the top- k ranking operation to regularized earth mover's problem by imposing entropy regularization to earth mover's distance. Then the regularized earth mover's problem can be solved with a Sinkhorn iteration [8] (in a differentiable manner) which enables gradient back-propagation effectively.

As in [87], [93], building correspondences based on semantic information only often leads to the losing of texture structures and patterns in warped exemplars. Thus, the spatial information should also be incorporated to preserve the texture structures and patterns and yield more accurate feature correspondences. A vanilla method to encode the position information is concatenating the semantic features with the corresponding feature coordinates via coordconv [40]. However, the vanilla position encoding builds a single coordinate system for the whole image which ignores the position information within each semantic region. Instead, we design a semantic position encoding (SPE) mechanism that builds

a dedicated coordinate system for each semantic region which outperforms the vanilla position encoding significantly.

In addition, conditional inputs and exemplars are seldom perfectly matched, e.g., conditional inputs could contain several semantic classes that do not exist in exemplar images. Under such circumstance, the built correspondences often contain errors which lead to inaccurate exemplar warping and further deteriorated image generation. We tackle this problem by designing a CONfidence Feature Injection (CONFI) module that fuses features of conditional inputs and warped exemplars according to the reliability of the built correspondences. Although the warped exemplar may not be reliable, the conditional input always provides accurate semantic guidance in image generation. The CONFI module thus assigns higher weights to the conditional input when the built correspondence (or warped exemplar) is unreliable. Experiments show that CONFI helps to generate faithful yet high-fidelity images consistently by assigning adaptive weights (to the conditional input) based on the reliability of the built correspondence.

The contributions of this work can be summarized in four aspects. First, we propose a versatile image translation and manipulation framework which introduces a bi-level feature alignment strategy that greatly reduces the memory cost while building the correspondence between conditional inputs and exemplars. Second, we approximate non-differentiable top- k ranking to a regularized earth mover's problem, which enables effective gradient propagation for end-to-end network training. Third, we introduce a semantic position encoding mechanism that encodes region-level position information to preserve texture structures and patterns. Fourth, we design a confidence feature injection module that provides reliable feature guidance in image translation and manipulation.

2 RELATED WORK

2.1 Image-to-Image Translation

Image translation has achieved remarkable progress in learning the mapping among images of different domains. It could be applied in different tasks such as style transfer [13], [22], [36], image super-resolution [31], [32], [38], [86], domain adaptation [19], [51], [57], [62], [77], [80], image synthesis [7], [73], [74], [75], [76], [79], [81], [82], [83], [84], image inpainting [39], [66], [71], [72], etc. To achieve high-fidelity and flexible translation, existing work uses different conditional inputs such as semantic segmentation [25], [54], [65], scene layouts [35], [59], [89], key points [11], [48], [50], edge maps [12], [25], etc. However, effective style control remains a challenging task in image translation.

Style control has attracted increasing attention in image translation and generation. Earlier works such as [30] regularize the latent feature distribution to control the generation outcome. However, they struggle to capture the complex textures of natural images. Style encoding has been studied to address this issue. For example, [23] and [47] transfer style codes from exemplars to source images via adaptive instance normalization (AdaIN) [22]. [5] employs a style encoder for style consistency between exemplars and translated images. [95] designs semantic region-adaptive normalization (SEAN) to control the style of each semantic region individually. Wang *et al.* [64] demonstrate the feasibility of exemplar-guided style control by directly concatenating exemplar image and condition as input for image translation. However, encoding style exemplars tends to capture the overall image style and ignores the texture details in local regions. To

achieve accurate style guidance for each local region, Zhang *et al.* [87] build dense semantic correspondences between conditional inputs and exemplars with Cosine similarity to capture accurate exemplar details. To mitigate the issue of many-to-one matching in Zhang *et al.* [87], Zhan *et al.* [78] further propose to utilize the mass preserving property of optimal transport to build the correspondence. On the other hand, above methods usually work with low-resolution correspondences due to the quadratic complexity in correspondence computation. To build correspondence in high resolution, Zhou *et al.* [93] introduce the GRU-assisted Patch-Match to efficiently establish the high-resolution correspondence. Zheng *et al.* [90] tackle the high-resolution correspondences through a sparse attention module with applications to semantic image manipulation. However, all these methods only utilize semantic information for building correspondence, which often leads to destroyed texture structures and patterns in the warped exemplar. In this work, we propose a bi-level alignment strategy that allows to build correspondence efficiently and design a semantic position encoding to preserve the texture structures and patterns.

2.2 Semantic Image Editing

The arise of generative adversarial network (GANs) brings revolutionary advance to image editing [4], [20], [52], [55], [67], [68], [94]. As one of the most intuitive representation in image editing, semantic information has been extensively investigated in conditional image synthesis. For example, Isola *et al.* [25] achieve label-to-pixel generation by training an encoder-decoder network with a conditional adversarial objective. Wang *et al.* [65] further achieve high-resolution image manipulation by editing the pixel-wise semantic labels. Park *et al.* [54] introduce spatially-adaptive normalization (SPADE) to inject guided features in image generation. MaskGAN [33] exploits a dual-editing consistency as auxiliary supervision for robust face image manipulation. Gu *et al.* [14] learn facial embeddings for different face components to enable local facial editing. Chen *et al.* [3] propose a mask re-targeting strategy for identity-preserved face animation. Xia *et al.* [69] map images into the latent space of a pre-trained network to facilitate editing. Instead of directly learning a label-to-pixel mapping, Hong *et al.* [20] propose a semantic manipulation framework HIM that generates images guided by a predicted semantic layout. Upon this work, Ntavelis *et al.* [52] propose SESAME which requires only local semantic maps to achieve image manipulation. However, the aforementioned methods either only learn a global feature without local focus (e.g., MaskGAN [33]) or ignore the features in the editing regions of the original image (e.g., HIM [20], SESAME [52]). To better utilize the fine features in the original image, Zheng *et al.* [90] adapt exemplar-based image synthesis framework CoCosNet [87] for semantic image manipulation by building a high-resolution correspondence between the original image and the edited semantic map. However, it may inherit the issue of texture pattern losing from [87], which can be effectively ameliorated by the proposed semantic positional encoding mechanism.

2.3 Feature Correspondence

Early studies determine feature correspondence by focusing on sparse correspondence [44] or dense correspondences between nearby view of the same objects only [21], [53]. Differently, semantics correspondences establish the dense correlation between different instances of the same semantic object. For example, [2],

[24], [29] focus on matching hand-crafted features. Leveraging the power of convolutional neural networks (CNNs) in learning high-level semantic features, Long *et al.* [43] first employ CNNs to establish semantic correspondences between images. Later efforts further improve correspondence quality by including additional annotations [6], [15], [16], [92], adopting coarse-to-fine strategy [37], extending to cross-domain images [87], etc. However, most existing studies only work with low-resolution correspondences as constrained by the heavy computation cost. We design a bi-level alignment strategy that greatly improves computation efficiency and allows to compute dense correspondences at higher resolution.

3 PROPOSED METHOD

The proposed RABIT consists of an alignment network and a generation network that are inter-connected as shown in Fig. 2. The alignment network learns the correspondence between a conditional input and an exemplar for warping the exemplar to be aligned with the conditional input. The generation network produces the final generation under the guidance of the warped exemplar and the conditional input. RABIT is typically applicable in the task of conditional image translation with extra exemplar as style guidance. It is also applicable to the task of image manipulation by treating the exemplars as the original images for editing and the conditional inputs as the edited semantic.

3.1 Alignment Network

The alignment network aims to build the correspondence between conditional inputs and exemplars, and accordingly provide accurate style guidance by warping the exemplars to be aligned with the conditional inputs. As shown in Fig. 2, conditional input and exemplar are fed to feature extractors F_X and F_Z to extract two sets of feature vectors $X = [x_1, \dots, x_L] \in \mathbb{R}^d$ and $Z = [z_1, \dots, z_L] \in \mathbb{R}^d$, where L and d denote the number and dimension of feature vectors, respectively. Most existing methods [17], [85], [87] align X and Z by building a $L \times L$ dense correspondence matrix where each entry denotes the Cosine similarity between the corresponding feature vectors in X and Z . However, such correspondence computation has quadratic complexity which incurs large memory and computation costs. Most existing studies thus work with low-resolution exemplar images (e.g. 64×64 in CoCosNet [87]) which often struggle in generating realistic images with fine texture details.

In this work, we propose a bi-level alignment strategy via a novel ranking and attention scheme (RAS) that greatly reduces computational costs and allows to build correspondences with high-resolution images as shown in Fig. 4. Instead of building correspondences between features directly, the bi-level alignment strategy builds the correspondences at two levels, including the first level that introduces top- k ranking to generate block-wise ranking matrices dynamically and the second level that achieves dense attention between the features within blocks. As Fig. 2 shows, b local features are grouped into a block, thus the features of conditional input and exemplar are partitioned into N blocks ($N = L/b$) as denoted by $X = [X_1, \dots, X_N] \in \mathbb{R}^{bd}$ and $Z = [Z_1, \dots, Z_N] \in \mathbb{R}^{bd}$. In the first level of top- k ranking, each block feature of the conditional input serves as a query to retrieve top- k block features from the exemplar according to the Cosine similarity between blocks. In the second level of local attention, the features in each query block further attends to the features in the top- k retrieved blocks to build up local attention matrices

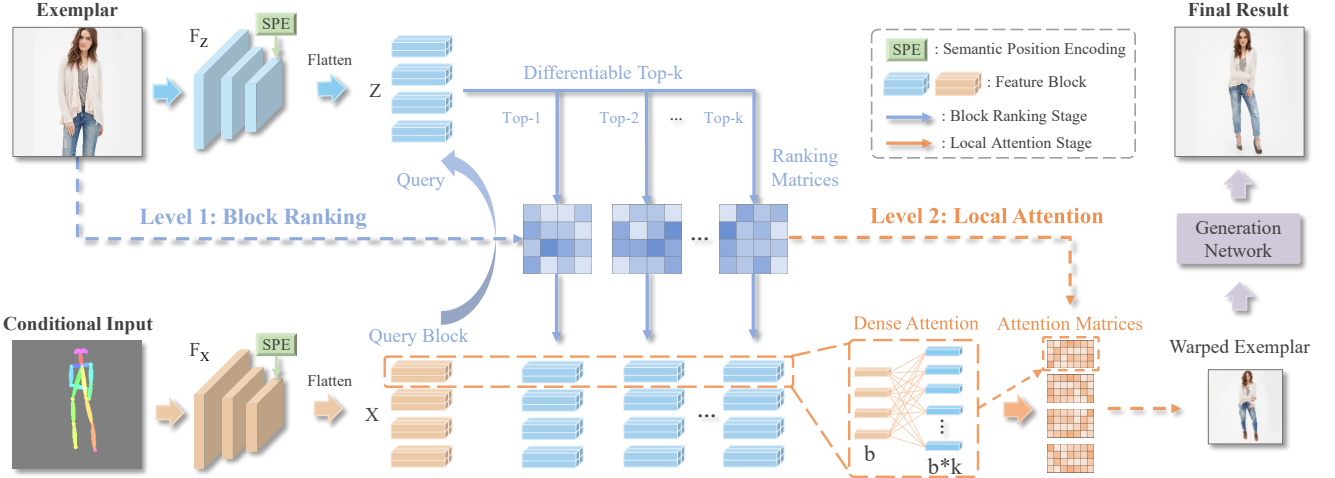


Fig. 2. The framework of the proposed RABIT: *Conditional Input* and *Exemplar* are fed to feature extractors F_X and F_Z to extract feature vectors X and Z where b local features form a feature block. In the first level, each block from the conditional input serves as the query to retrieve top- k similar blocks from the exemplar through a differentiable ranking operation. In the second level, *dense Attention* is then built between the b features in query block and $b * k$ features in the retrieved blocks. The built *Ranking Matrices* and *Attention Matrices* are combined to warp the exemplar to be aligned with the conditional input as in *Warped Exemplar*, which serves as a style guidance to generate the final result through a generation network.

within block features. The correspondence between the exemplar and conditional input can thus be built much more efficiently by combining such inter-block ranking and inner-block attention.

Semantic Position Encoding. Existing works [87], [93] mainly rely on semantic features to establish the correspondences. However, as all textures within a semantic region share the same semantic feature, the pure semantic correspondence fails to preserve the texture structures or patterns within each semantic region. For example, the building regions of conditional inputs in Fig. 4 will establish correspondence with the building regions in the exemplars without consideration of building textures, which will result in warped exemplars with messy textures as shown in the Baseline (64). Thus, the position information of features should also be facilitated to preserve the texture structures and patterns. A vanilla method to encode the position information is employing a simple coordconv [40] to build a global coordinate for the full image. However, this vanilla position encoding mechanism builds a single coordinate system for the whole image, ignoring region-wise semantic differences. To preserve the fine texture pattern within each semantic region, we design a semantic position encoding (SPE) mechanism that builds a dedicated coordinate for each semantic region as shown in Fig. 3. Specifically, SPE treats the center of each semantic region as the origin of coordinate, and the coordinates within each semantic region are normalized to $[-1, 1]$. The proposed SPE outperforms the vanilla position encoding significantly as shown in Fig. 4 and to be evaluated in experiments.

3.2 Differentiable Top- k Ranking

The core of the ranking and attention scheme lies with a top- k operation that ranks the correlative blocks. However, the original top- k operation involves index swapping whose gradient cannot be computed and so cannot be integrated into end-to-end network training. We tackle this issue by formulating the top- k ranking as a regularized earth mover's problem which allows gradient computation via implicit differentiation [46], [70].

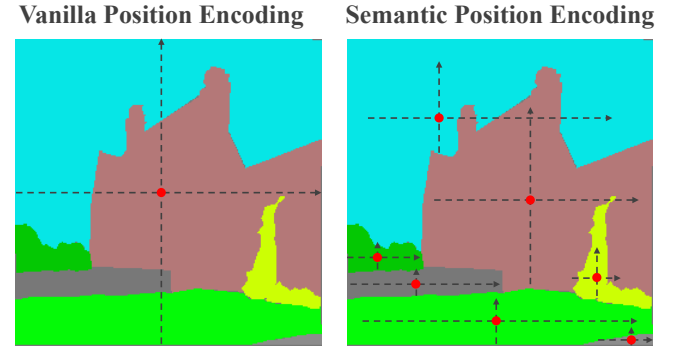


Fig. 3. The comparison of vanilla position encoding and the proposed semantic position encoding (SPE). Red dots denote the coordinate origin. The proposed SPE builds dedicated coordinate for each semantic region.

3.2.1 Top- k Ranking Formulation

We first show that a specific form of earth mover's problem is essentially equivalent to a top- k element ranking problem. Earth mover's problem [27] aims to find a transport plan that minimizes the total cost to transform one distribution to another. Consider two discrete distributions $U = [\mu_1, \dots, \mu_N]^\top$ and $V = [\nu_1, \dots, \nu_M]^\top$ defined on supports $\mathcal{A} = [a_1, \dots, a_N]$ and $\mathcal{B} = [b_1, \dots, b_M]$, with probability (or amount of earth) $\mathbb{P}(a_i) = \mu_i$ and $\mathbb{P}(b_j) = \nu_j$. We define $C \in \mathbb{R}^{N \times M}$ as the cost matrix where C_{ij} denotes the cost of transportation between a_i and b_j , and T as a transport plan where T_{ij} denotes the amount of earth transported between μ_i and ν_j . An earth mover's (EM) problem can be formulated by:

$$\text{EM} = \min_T \langle C, T \rangle, \quad \text{s.t. } T \vec{1}_M = U, \quad T^\top \vec{1}_N = V. \quad (1)$$

where $\vec{1}$ denotes a vector of ones, $\langle \cdot \rangle$ denotes inner product.

We then derive the earth mover's form of top- k operator. With a query block from the conditional input and N blocks from the exemplar, their correlation scores $\mathcal{A} = [a_1, \dots, a_N]$, $a_i \in$

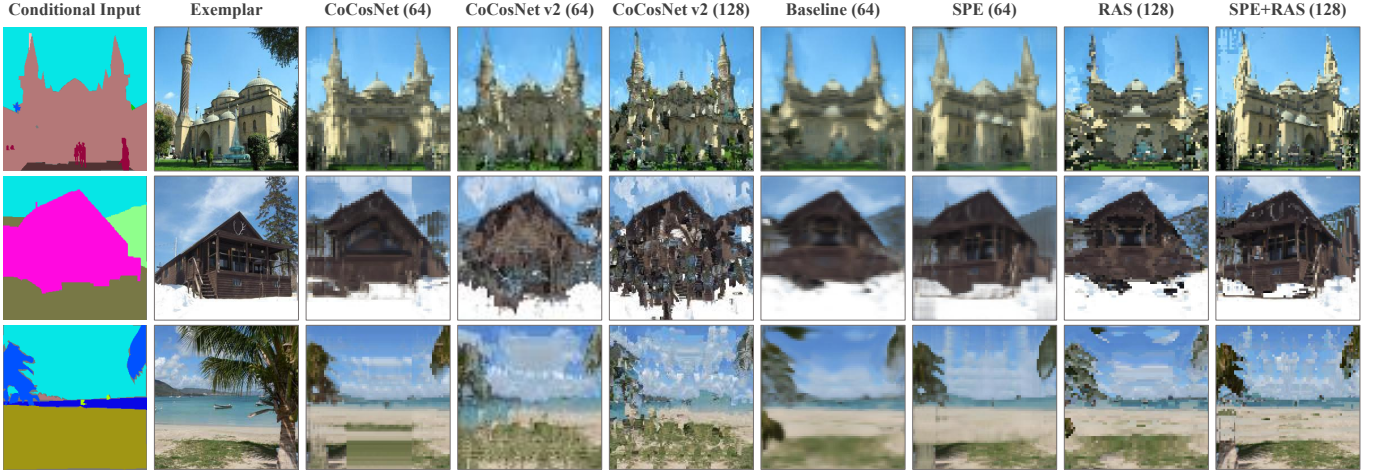


Fig. 4. Warped exemplars with different methods: '64' and '128' mean to build correspondences at resolutions 64×64 and 128×128 . CoCosNet [87] tends to lose texture details and structures, while CoCosNet v2 [93] tends to generate messy warping. The Baseline denotes building correspondences with Cosine similarity, which tends to lose textures details and structures. The proposed ranking and attention scheme (RAS) allows efficient image warping at high resolutions, the proposed semantic position encoding (SPE) can better preserve texture structures. The combination of the two as denoted by SPE+RAS achieves the best warping performance with high resolution and preserved texture structures.

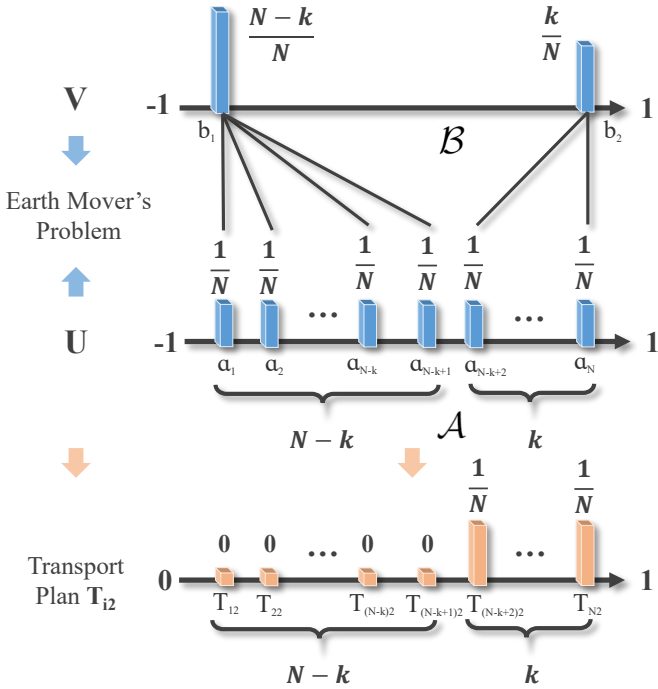


Fig. 5. Illustration of the earth mover's problem in top- k retrieval. Earth mover's problem is conducted between distributions U and V which is defined on supports $\mathcal{A} = [a_1, \dots, a_N]$ and $\mathcal{B} = [b_1, b_2]$. Transport Plan T_{i2} indicates the retrieved top- k elements.

$[-1, 1]$ can be obtained based on their Cosine similarity. The top- k operation aims to retrieve k most similar elements from \mathcal{A} . We define another set $\mathcal{B} = \{-1, 1\}$, and consider two discrete distributions $U = [\mu_1, \dots, \mu_N]$ and $V = [\nu_1, \nu_2]$ defined on supports sets \mathcal{A} and \mathcal{B} with $\mu_i = 1/N, i \in [1, N]$, $\nu_1 = (N - k)/N$ and $\nu_2 = k/N$. The cost C is defined to be the squared Euclidean distance, i.e., $C_{i1} = (a_i + 1)^2$ and $C_{i2} = (a_i - 1)^2, i \in [1, N]$. The earth mover's distance between

U and V can thus be formulated as:

$$\begin{aligned} \min_T \langle C, T \rangle &= \min_T \left\{ \sum_{i=1}^N \left[(a_i + 1)^2 T_{i1} + (a_i - 1)^2 T_{i2} \right] \right\} \\ &= \min_T \left\{ 2 \sum_{i=1}^N a_i (T_{i1} - T_{i2}) + \frac{1}{N} \sum_{i=1}^N a_i^2 + 1 \right\} \end{aligned}$$

Therefore minimizing $\langle C, T \rangle$ suffices to minimize $\sum_{i=1}^N a_i (T_{i1} - T_{i2})$. It is obvious that $\sum_{i=1}^N T_{i2} = \frac{k}{N}$, $\sum_{i=1}^N T_{i1} = \frac{N-k}{N}$ and $T_{i1} + T_{i2} = \frac{1}{N}$. Hence, minimizing $\sum_{i=1}^N a_i (T_{i1} - T_{i2})$ essentially aims to select the largest k elements from $\mathcal{A} = [a_1, \dots, a_N]$ as implied in the transport plan T :

$$T_{i1} = \begin{cases} 0 & a_i \in \text{top-}k \\ \frac{1}{N} & a_i \notin \text{top-}k \end{cases}, \quad T_{i2} = \begin{cases} \frac{1}{N} & a_i \in \text{top-}k \\ 0 & a_i \notin \text{top-}k \end{cases}$$

where T_{i2} indicates the retrieved top- k elements. Fig. 5 illustrates the earth mover's problem and transport plan, where the earth from the k closest points is transported to 1, and meanwhile the earth from the $N - k$ remaining points is transported to -1 . Therefore, the transport plan T exactly indicates the top- k elements.

3.2.2 Differentiable Optimization

The top- k operation has been formulated as an earth mover's problem, while the standard earth mover's problem cannot be solved in a differentiable way. We introduce a regularized earth mover's distance which serves as a smoothed approximation to the standard top- k operator, and enables effective gradient propagation. The regularized earth mover's problem in Eq. (1) is defined as:

$$\begin{aligned} \text{EM}_\epsilon &= \min_T \langle C, T \rangle + \epsilon H(T) \\ \text{s.t. } T \vec{1}_M &= U, T^\top \vec{1}_N = V \end{aligned} \quad (2)$$

where $H(T) = \sum_{i,j} T_{ij} \log T_{ij}$ is the regularization term, ϵ is the regularization coefficient. The optimal transport plan T_ϵ of the regularized earth mover's problem thus becomes a smoothed version of the standard top- k operator.

The regularized earth mover's distance can be efficiently computed via the Sinkhorn algorithm [8]. Specifically, an exponential kernel is applied to the cost matrix C which yields $C' = \exp(-\lambda C)$. Then C' is converted iteratively towards a doubly stochastic matrix through a Sinkhorn operation $\mathcal{S}(\cdot)$ as denoted by:

$$\mathcal{S}^m(C') = \begin{cases} C' & m = 0 \\ \mathcal{N}^c(\mathcal{N}^r(\mathcal{S}^{m-1}(C'))) & \text{otherwise} \end{cases}$$

where m denotes the iteration number, $\mathcal{N}^r(\cdot)$ and $\mathcal{N}^c(\cdot)$ are row and column normalization which can be denoted by:

$$\mathcal{N}_{ij}^r(C') = \frac{C'_{ij}}{\sum_{k=1}^2 C'_{ik}}, \quad \mathcal{N}_{ij}^c(C') = \frac{C'_{ij}}{\sum_{k=1}^N C'_{kj}},$$

where C'_{ij} represents an element in C' . Then the partial derivatives for the iteration (taking $m = 1$ as the example) can be derived by:

$$\frac{\partial \mathcal{S}^1}{\partial c'_{st}} = \frac{\partial \mathcal{N}_{st}^c}{\partial \mathcal{N}_{st}^r} \cdot \sum_{j=1}^2 \left[\frac{\mathbb{I}_j^t}{\sum_{k=1}^2 c'_{sk}} - \frac{c'_{sj}}{(\sum_{k=1}^2 c'_{sk})^2} \right]$$

where s and t, k, j represent the indices of the row and columns in C' , $\mathbb{I}_j^t = \begin{cases} 1 & \text{if } j = t \\ 0 & \text{otherwise} \end{cases}$ represents an indication function.

Thus, the Sinkhorn operation is differentiable and its gradient can be calculated by unrolling the sequence of the row and column normalization operations. When iterations converge, the transport plan $T_\epsilon = \mathcal{S}^m(C')$ indicating the top- k elements can be obtained.

3.2.3 Complexity Analysis

The vanilla dense correspondence has a self-attention memory complexity $\mathcal{O}(L^2)$ where L is the input sequence length. For our bi-level alignment strategy, the memory complexity of building the block ranking matrices and local attention matrices are $\mathcal{O}(N^2)$ and $\mathcal{O}(b * (kb))$, where b, N ($N = L/b$) and k are block size, block number and the number of top- k selection. Thus, the overall memory complexity of the proposed bi-level alignment strategy is $\mathcal{O}(N^2 + b * (kb))$.

3.3 Generation Network

The generation network aims to synthesize images under the semantic guidance of conditional inputs and style guidance of exemplars. As the exemplars are warped by the alignment network to be semantically matched with the conditional inputs, the warped exemplar can serve as accurate style guidance for each image region in the generation network. The overall architecture of the generation network is similar to SPADE [54]. Please refer to supplementary material for details of the network structure.

State-of-the-art approach [87] simply concatenates the warped exemplar and conditional input to guide the image generation process. However, conditional input and warped exemplar are from different domains with different distributions and a naive concatenation of them is often sub-optimal [9]. In addition, the warped input image and edited semantic map could be structurally aligned but semantically different especially when they have severe semantic discrepancy. Such unreliable warped exemplars could serve as false guidance for the generation network and heavily deteriorate the generation performance. Therefore, a mechanism is required to identify the semantic reliability of warped exemplar to provide reliable guidance for the generation network. To this end, we propose a CONfidence Feature Injection

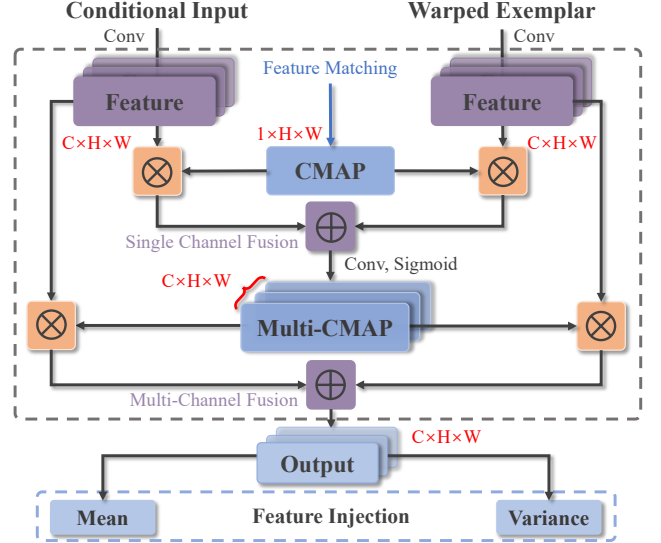


Fig. 6. Illustration of confidence feature injection: Conditional input and warped exemplar are initially fused with a confidence map (CMAP) of size $1 \times H \times W$. A multi-channel confidence map (Multi-CMAP) of size $C \times H \times W$ is then obtained from the initial fusion which further fuses the conditional input and warped exemplar in multiple channels.

(CONFI) module that adaptively weights the features of conditional input and warped exemplar according to the reliability of feature matching.

Confidence Feature Injection. Intuitively, in the case of lower reliability of the feature correspondence, we should assign a relatively lower weight to the warped exemplar which provides unreliable style guidance and a higher weight to the conditional input which consistently provides accurate semantic guidance.

As illustrated in Fig. 6, the proposed CONFI fuses the features of the conditional input and warped exemplar based on a confidence map (CMAP) that captures the reliability of the feature correspondence. To derive the confidence map, we first obtain a block-wise correlation map of size $N \times N$ by computing element-wise Cosine distance between $X = [X_1, \dots, X_N]$ and $Z = [Z_1, \dots, Z_N]$. For a block X_i , the correlation score with Z is denoted by $\mathcal{A} = [a_1, \dots, a_N]$. As higher correlation scores indicate more reliable feature matching, we treat the peak value of \mathcal{A} as the confidence score of X_i . Similar for other blocks, we can obtain the confidence map (CMAP) of size $1 \times H \times W$ ($N = H * W$) which captures the semantic reliability of all blocks. The features of the conditional input and exemplar (both of size $C \times H \times W$ after passing through convolution layers) can thus be fused via weighted sum based on the confidence map CMAP:

$$F = X * (1 - \text{CMAP}) + (T \cdot Z) * \text{CMAP}$$

where T is the built correspondence matrix.

As the confidence map contains only one channel ($1 \times H \times W$), the above feature fusion is conducted in $H \times W$ but ignores that in C channel. To achieve thorough feature fusion in all channels, we feed the initial fusion F to convolution layers to generate a multi-channel confidence map (Multi-CMAP) of size $C \times H \times W$. The conditional input and warped exemplar are then thoroughly fused via a full channel-weighted summation according to the Multi-CMAP. The final fused feature is further injected to the

TABLE 1
Comparing RABIT with state-of-the-art image translation methods over four translation tasks with FID, SWD and LPIPS as the evaluation metrics.

Methods	ADE20K			CelebA-HQ (Semantic)			DeepFashion			CelebA-HQ (Edge)		
	FID \downarrow	SWD \downarrow	LPIPS \uparrow	FID \downarrow	SWD \downarrow	LPIPS \uparrow	FID \downarrow	SWD \downarrow	LPIPS \uparrow	FID \downarrow	SWD \downarrow	LPIPS \uparrow
Pix2pixHD [65]	81.80	35.70	N/A	43.69	34.82	N/A	25.20	16.40	N/A	42.70	33.30	N/A
StarGAN v2 [5]	98.72	65.47	0.551	53.20	41.87	0.324	43.29	30.87	0.296	48.63	41.96	0.214
SPADE [54]	33.90	19.70	0.344	39.17	29.78	0.254	36.20	27.80	0.231	31.50	26.90	0.207
SelectionGAN [61]	35.10	21.82	0.382	42.41	30.32	0.277	38.31	28.21	0.223	34.67	27.34	0.191
SMIS [96]	42.17	22.67	0.476	28.21	24.65	0.301	22.23	23.73	0.240	23.71	22.23	0.201
SEAN [95]	24.84	10.42	0.499	17.66	14.13	0.285	16.28	17.52	0.251	16.84	14.94	0.203
CoCosNet [87]	26.40	10.50	0.580	21.83	12.13	0.292	14.40	17.20	0.272	14.30	15.30	0.208
CoCosNet v2 [93]	25.20	9.900	0.557	20.64	11.21	0.303	13.04	16.65	0.270	13.21	14.01	0.216
RABIT	24.35	9.893	0.571	20.44	11.18	0.307	12.58	16.03	0.284	11.67	14.22	0.219

TABLE 2

Comparing RABIT with state-of-the-art image translation methods in semantic consistency and style consistency (on ADE20K [91]).

Methods	Semantic Consistency		Style Consistency	
	VGG ₄₂ \uparrow	VGG ₅₂ \uparrow	VGG _M \uparrow	VGG _V \uparrow
SPADE [54]	0.861	0.772	0.934	0.884
StarGAN v2 [5]	0.741	0.718	0.919	0.907
SelectionGAN [61]	0.843	0.785	0.951	0.912
SMIS [96]	0.862	0.787	0.951	0.933
SEAN [95]	0.868	0.791	0.962	0.942
CoCosNet [87]	0.878	0.790	0.986	0.965
CoCosNetv2 [93]	0.889	0.800	0.994	0.972
RABIT	0.891	0.812	0.993	0.977

generation process via spatial de-normalization [54] to provide accurate semantic and style guidance.

3.4 Loss Functions

The alignment network and generation network are jointly optimized. For clarity, we still denote the conditional input and exemplar as X and Z , the ground truth as X' , the generated image as Y , the feature extractors for conditional input and exemplar as E_X and E_Z , the generator and discriminator in the generation network as G and D .

Alignment Network. First, the warping should be cycle consistent, i.e. the exemplar should be recoverable from the warped warped. We thus employ a cycle-consistency loss as follows:

$$\mathcal{L}_{cyc} = \|T^\top \cdot T \cdot Z - Z\|_1$$

where T is the correspondence matrix. The feature extractors F_X and F_Z aim to extract invariant semantic information across domains, i.e. the extracted features from X and X' should be consistent. A feature consistency loss can thus be formulated as follows:

$$\mathcal{L}_{cst} = \|F_X(X) - F_Z(X')\|_1$$

Generation Network. The generation network employs several losses for high-fidelity synthesis with consistent style with the exemplar and consistent semantic with the conditional input. As the generated image Y should be semantically consistent with the ground truth X' , we employ a perceptual loss \mathcal{L}_{perc} [26] to penalize their semantic discrepancy as below:

$$\mathcal{L}_{perc} = \|\phi_l(Y) - \phi(X')\|_1 \quad (3)$$

where ϕ_l is the activation of layer l in pre-trained VGG-19 [58] model. To ensure the statistical consistency between the generated image Y and the exemplar Z , a contextual loss [49] is adopted:

$$\mathcal{L}_{cxt} = -\log(\sum_i \max_j CX_{ij}(\phi_l^i(Z), \phi_l^j(Y))) \quad (4)$$

where i and j are the indexes of the feature map in layer ϕ_l . Besides, a pseudo pairs loss \mathcal{L}_{pse} as described in [87] is included in training.

The discriminator D is employed to drive adversarial generation with an adversarial loss \mathcal{L}_{adv} [25]. The full network is thus optimized with the following objective:

$$\mathcal{L} = \min_{F_X, F_Z, G} \max_D (\lambda_1 \mathcal{L}_{cyc} + \lambda_2 \mathcal{L}_{cst} + \lambda_3 \mathcal{L}_{perc} + \lambda_4 \mathcal{L}_{cxt} + \lambda_5 \mathcal{L}_{pse} + \lambda_6 \mathcal{L}_{adv}) \quad (5)$$

where the weights λ balance the losses in the objective.

4 EXPERIMENTS

4.1 Experimental Settings

Datasets: We evaluate and benchmark our method over multiple datasets for image translation & manipulation tasks.

- ADE20K [91] has 20k training images each of which is associated with a 150-class segmentation mask. We use its semantic segmentation as conditional inputs in image translation experiments, and 2k test images for evaluations. For image manipulation, we apply object-level affine transformations on the test set to acquire paired data (150 images) for evaluations as in [90].

- CelebA-HQ [42] has 30,000 high-quality face images. We conduct two translation tasks by using face semantics and face edges as conditional inputs. In addition, we also conduct image manipulation experiments on this dataset by editing the face semantics. We use 2993 face images for translation evaluations as in [87], and manually edit 100 semantic maps which is randomly selected for image manipulation evaluations.

- DeepFashion [41] has 52,712 person images of different appearance and poses. We use its key points as conditional inputs for image translation, and select 4993 images for evaluations as in [87].

Evaluation Metrics: For image translation, we adopt *Fréchet Inception Score (FID)* [18] and *Sliced Wasserstein distance (SWD)* [28] to evaluate the perceptual quality of translated images. We adopt *Learned Perceptual Image Patch Similarity (LPIPS)* [88] to evaluate the translation diversity with different exemplars.

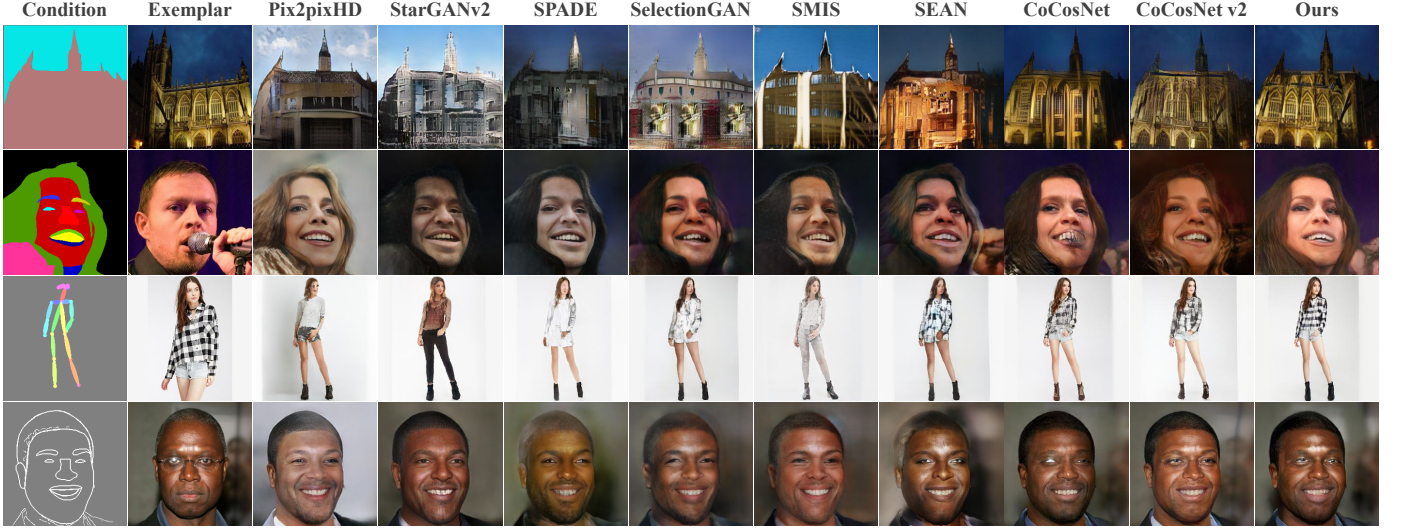


Fig. 7. Qualitative comparison of the proposed RABIT and state-of-the-art methods over four types of conditional image translation tasks.

For image manipulation, we adopted FID, SWD and LPIPS to evaluate perceptual quality of manipulated images. We also adopted L1 distance, peak signal-to-noise ratio (PSNR) and structural similarity index (SSIM) as low-level evaluation metrics. Note LPIPS evaluates image translation diversity by measuring the distance between translated images, while it evaluates the image manipulation quality by measuring the distance between manipulated images and ground truth.

Similar to [87], we design VGG₄₂ and VGG₅₂ metrics to evaluate semantic consistency and VGG_M and VGG_V metrics to evaluate style consistency. For semantic consistency, we apply a pre-trained VGG model [58] to extract high-level features (*relu4_2* and *relu5_2*) of the ground truth and generated images. The semantic consistency (VGG₄₂ and VGG₅₂) is defined by the distance between the extracted high-level features as computed by Cosine similarity. For style consistency, we extract low-level style features (*relu1_2*) from the generated images and exemplars. The style consistency (VGG_M and VGG_V) is defined by the distance of channel-wise mean and standard deviation as computed by Cosine similarity.

Implementation Details: The alignment and generation networks are jointly optimized with learning rates $1e-4$ and $4e-4$ for the generator and discriminator, respectively. We adopted Adam solver with $\beta_1 = 0$ and $\beta_2 = 0.999$. All experiments were conducted on 4 32GB Tesla V100 GPUs with synchronized BatchNorm. The default size for our correspondence computation is 128×128 with a block size of 2×2 . The number k in top- k ranking is set at 3 by default in our experiments. The size of generated images is 256×256 in all generation tasks.

4.2 Image Translation Experiments

We compare RABIT with eight state-of-the-art image translation methods: 1) Pix2pixHD [65] on supervised image translation; 2) StarGAN v2 [5] on multi-modal translation with support for style encoding from reference images; 3) SPADE [54] on supervised translation that supports style injection from exemplar images; 4) SelectionGAN [61] on guided translation with cascaded semantic guidance; 5) SMIS [96] on semantically multi-modal synthesis with all group convolutions; 6) SEAN [95] on conditional generation that can control the style of each individual semantic region;

7) CoCosNet [87] on exemplar-based image translation that builds cross-domain correspondences; and 8) CoCosNet v2 [93] on building high-resolution correspondences for image translation. Note CoCosNet adopts a default correspondence size of 64×64 in this work as constrained by high memory costs, whereas CoCosNet v2 and RABIT adopt a default correspondence size of 128×128 .

Quantitative Results. In quantitative experiments, all methods translate images with the same exemplars except Pix2PixHD [65] which doesn't support style injection from exemplars. LPIPS is calculated by comparing the generated images with randomly selected exemplars. All compared methods adopt three exemplars for each conditional input and the final LPIPS is obtained by averaging the LPIPS between any two generated images.

Table 1 shows experimental results. It can be seen that RABIT outperforms all compared methods over most metrics and tasks consistently. By building explicit yet accurate correspondences between conditional inputs and exemplars, RABIT enables direct and accurate guidance from the exemplar and achieves better translation quality (in FID and SWD) and diversity (in LPIPS) as compared with the regularization-based methods such as SPADE [54] and SMIS [96], and style-encoding methods such as StarGAN v2 [5] and SEAN [95]. Compared with correspondence-based method CoCosNet [87], the proposed bi-level alignment allows RABIT to build correspondences and warp exemplars at higher resolutions (e.g. 128×128) which offers more detailed guidance in the generation process and helps to achieve better FID and SWD. While compared with CoCosNet v2 [93], the proposed semantic position encoding enables to preserve the texture structures and patterns, thus yielding more accurate warped exemplars as guidance. In addition, the proposed confidence feature injection module fuses conditional inputs and warped exemplars adaptively based on the matching confidence, which provides more reliable guidance and improves FID and SWD. Besides generation quality, RABIT achieves the best generation diversity in LPIPS except StarGAN v2 [5] which sacrifices the generation quality with much lower FID and SWD.

We also evaluated the generated images by measuring their semantic consistency with the conditional inputs and their style consistency with the exemplars. As shown in Table 2, the proposed RABIT achieves the best style consistency thanks to the bi-level

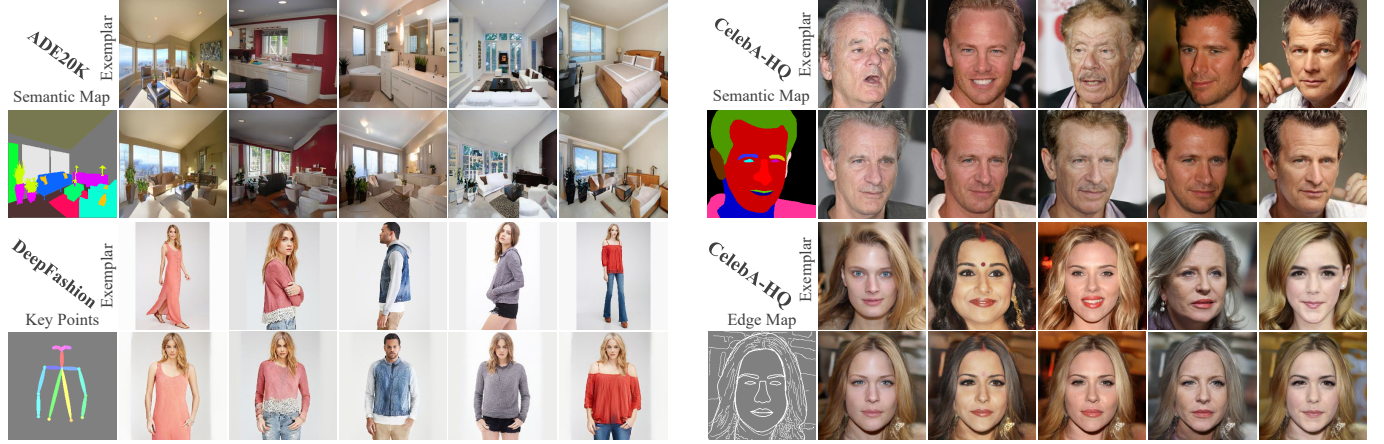


Fig. 8. Illustration of generation diversity of the proposed RABIT: With the same conditional input, RABIT can generate a variety of images that have consistent styles with the provided exemplars. It works for different types of conditional inputs consistently.

TABLE 3
Comparing RABIT with state-of-the-art image manipulation methods on ADE20K [91] with evaluation metrics FID, SWD, PSNR, and SSIM.

Models	FID \downarrow	SWD \downarrow	PSNR \uparrow	SSIM \uparrow
SPADE [54]	120.2	41.62	13.11	0.334
HIM [20]	59.89	22.23	18.23	0.667
SESAME [52]	52.51	29.40	18.67	0.691
CoCosNet [87]	41.03	23.08	20.30	0.744
CoCosNetv2 [93]	34.31	19.55	21.75	0.797
RABIT	26.61	15.05	23.08	0.823

TABLE 4
Comparing RABIT with state-of-the-art image manipulation methods on CelebA-HQ [42] with evaluation metrics FID, SWD, SSIM.

Models	FID \downarrow	SWD \downarrow	LPIPS \downarrow
SPADE [54]	105.1	41.90	0.376
SEAN [95]	96.31	35.90	0.351
MaskGAN [33]	80.89	23.86	0.271
CoCosNet [87]	68.70	22.90	0.224
CoCosNetv2 [93]	62.53	21.11	0.190
RABIT	60.87	21.07	0.176

feature alignment for building high-resolution correspondences and the semantic position encoding for preservation of texture patterns. It also achieves the best semantic consistency due to the confidence feature injection that offers reliable fusion of semantic and style features.

Qualitative Evaluations. Fig. 7 shows qualitative comparisons. It can be seen that RABIT achieves the best visual quality with faithful styles as exemplars. SPADE [54], SMIS [96] and StarGAN v2 [5] adopt single latent code to encode image styles, which tend to capture global styles but miss local details. SEAN [95] employs multiple latent codes but struggles in preserving faithful exemplar styles. CoCosNet [87] builds low-resolution correspondences which leads to missing details, while CoCosNet v2 [93] builds high-resolution correspondence without position encoding which leads to destroyed texture patterns. RABIT excels with its RAS that offers accurate feature alignment at high

TABLE 5
Comparing RABIT with state-of-the-art image manipulation methods in semantic consistency and style consistency (on ADE20K [91]).

Methods	Semantic Consistency		Style Consistency	
	VGG ₄₂ \uparrow	VGG ₅₂ \uparrow	VGG _M \uparrow	VGG _V \uparrow
SPADE [54]	0.853	0.766	0.929	0.876
HIM [20]	0.865	0.773	0.934	0.884
SESAME [52]	0.870	0.779	0.969	0.947
CoCosNet [87]	0.878	0.790	0.986	0.965
CoCosNet v2 [93]	0.889	0.804	0.985	0.967
RABIT	0.889	0.802	0.992	0.975

resolution and SPE that preserves texture structures and patterns.

RABIT also demonstrates superior diversity in image translation as illustrated in Fig. 8. It can be observed that RABIT is capable of synthesizing various high-fidelity images with faithful styles as various exemplars.

4.3 Image Manipulation Experiment

The proposed RABIT manipulates images by treating input images as exemplars and edited semantic guidance as conditional inputs. We compare RABIT with several state-of-the-art image manipulation methods including 1) SPADE [54], which supports semantic manipulation with style injection from input images; 2) SEAN [95] which supports semantic manipulation with style control of each individual semantic region; 3) MaskGAN [34], a geometry-oriented face manipulation framework with semantic masks as an intermediate representation for manipulation. 4) Hierarchical Image Manipulation (HIM) [20], a hierarchical framework for semantic image manipulation. 5) SESAME [52], a semantic image editing method covering the operation of adding, manipulating, and erasing. 6) CoCosNet [87], a leading exemplar-based image generation framework that enables manipulation by building cross-domain correspondences. 7) CoCosNet v2 [93], which builds high-resolution correspondences (128×128) for image generation.

Quantitative Results: In quantitative experiments, all compared methods manipulate images with the same input image and edited semantic label map. Table 3 shows experimental results over the synthesized test set of ADE20K [91]. It can be observed that RABIT outperforms state-of-the-art methods over all evalua-



Fig. 9. Qualitative illustration of RABIT and state-of-the-art image manipulation methods on the augmented test set of ADE20K with ground truth as described in [90]: The edited regions of the semantic maps are highlighted by white boxes. The artifacts generated by CoCosNet and CoCosNet v2 are highlighted by orange boxes. The proposed RABIT is capable of generating high-fidelity editing results without undesired artifacts.



Fig. 10. The comparison of image manipulation by MaskGAN [33] and the proposed RABIT over dataset CelebA-HQ [42].

tion metrics consistently. Table 4 shows experimental results over the CelebA-HQ dataset with manual edited semantic maps. It can be observed that RABIT outperforms the state-of-the-art methods by large margins in all perceptual quality metrics. The superior generation quality of RABIT is largely attributed to the ranking and attention scheme for building high-resolution correspondences and the semantic position encoding for preserving rich texture details of input images.

Besides the quality of manipulated images, we also evaluate their semantic consistency and style consistency as shown in Table 5. It can be seen that RABIT achieves the best semantic consistency and style consistency as compared with state-of-the-art image manipulation methods. The outstanding performance can be explained by the proposed ranking and attention scheme for building high-resolution correspondence, the semantic position encoding for texture pattern preservation as well as the confidence feature injection for reliable image generation.

Qualitative Evaluation: Fig. 9 shows visual comparisons with state-of-art manipulation methods on ADE20K. HIM [20] and SESAME [52] produce unrealistic texture and artifacts for drastic semantic changes due to the lack of texture details after

masking. CoCosNet [87] can preserve certain details, but it adopts Cosine similarity to align low-resolution features which often lead to missing details as demonstrated by blurry textures and artifacts. RABIT achieves superior fidelity due to its bi-level feature alignment for building high-resolution correspondences, semantic position encoding for the preservation of texture patterns and confidence feature injection for reliable guidance in image generation. Fig. 11 shows the editing capacity of RABIT with various types of manipulation on semantic labels. It can be seen that the RABIT manipulation results faithfully aligns with the edited semantic maps and produces realistic details. With the proposed bi-level feature alignment strategy and semantic position encoding, RABIT accurately matches features for the edited semantics and minimizes undesired changes outside the editing regions.

We also compare RABIT with MaskGAN [33] on CelebA-HQ [34] in Fig. 10. MaskGAN tends to introduce undesired changes in the edited images such as the skin color (columns 1 and 3) and the missing hand (column 2). RABIT achieves better editing with little change in other regions due to the accurate correspondences built between input images and edited semantic maps.

4.4 User Study

We conduct crowdsourcing user studies through Amazon Mechanical Turk (AMT) to evaluate the image translation & manipulation in terms of generation quality and style consistency. The code of the AMT user studies is available at ¹. Specifically, each compared method generates 100 images with the same conditional inputs and exemplars. Then the generated images together with the conditional inputs and exemplars were presented to 10 users for assessment. For the evaluation of image quality, the users were instructed to pick the best-quality images. For the evaluation of style consistency, the users were instructed to select the images with best style relevance to the exemplar. The final AMT score is the averaged number of the methods to be selected as the best quality and the best style relevance.

1. <https://github.com/fnzhan/AMT>

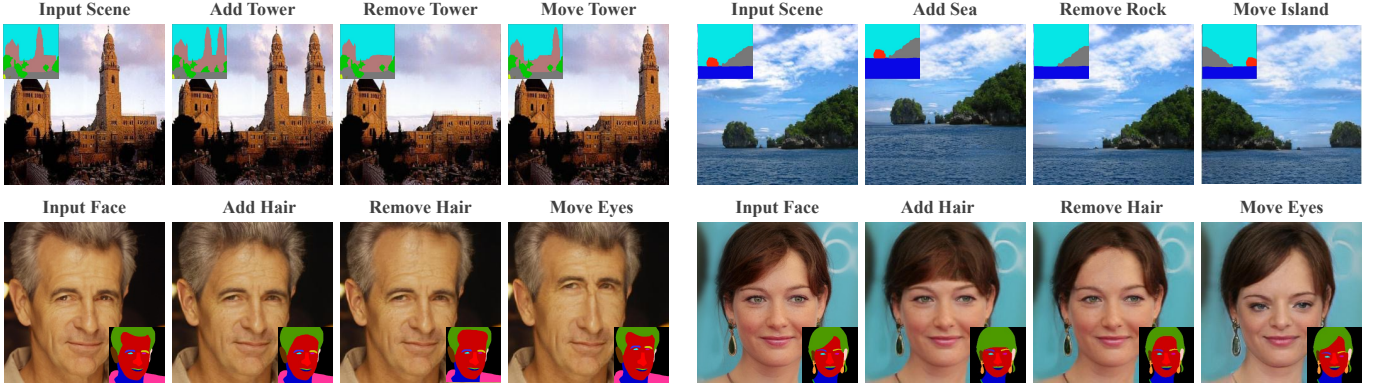


Fig. 11. Various image editing by the proposed RABIT: With input images as the exemplars and edited semantic maps as the conditional input, RABIT generates new images with faithful semantics and high-fidelity textures with little artifacts.

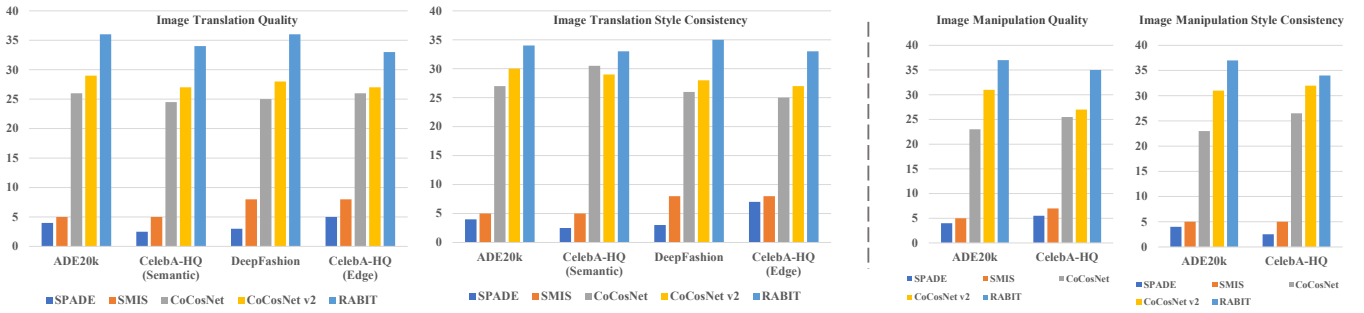


Fig. 12. AMT (Amazon Mechanical Turk) user studies of different image translation and image manipulation methods in terms of the visual quality and style consistency of the generated images.

Fig. 12 shows AMT results on multiple datasets. It can be observed that RABIT outperforms state-of-the-art methods consistently in image quality and style consistency on both image translation & image manipulation tasks.

4.5 Ablation Study

We conduct extensive ablation studies to evaluate our technical designs on image translation and image manipulation tasks. Table 6 shows experimental results on ADE20K. SPADE [54] is selected as the baseline which achieves image translation & manipulation without feature alignment. The performance is clearly improved when Cosine similarity is included to align features as denoted by (SPADE+COS). By replacing SPADE with the proposed CONFI for feature injection, the FID score is improved to 15.97. In addition, the translation is further improved by large margins when the proposed RAS is included for building high-resolution correspondences. By including vanilla position encoding (PE), FID score presents some improvement but VGG_{52} scores (semantic consistency) is affected severely. The proposed semantic position encoding improves FID scores and semantic consistency consistently.

As the correspondence quality is critical to correspondence-based generation, we analyze the accuracy, memory costs and parameters (e.g., resolution, block size) in correspondence construction in different methods. The experiment was conducted on DeepFashion dataset [41] (with paired images) where the warped exemplars and the ground truth (resized to 256×256) are compared in L1, SSIM and PSNR metrics to evaluate the accuracy of built correspondences. The memory cost is evaluated

through the memory footprint in GPU. In experiments, we compare Cosine similarity, Patch match and the proposed RAS over sizes of 64×64 , 128×128 and 128×128 , respectively. As shown in Table 7, RAS($k=3, b=4$) outperforms Cosine similarity in CoCosNet [87] and Patch match in CoCosNet v2 [93] in L1, SSIM and PSNR. In addition, RAS($k=1, b=64$) reduces memory costs consistently under different image resolutions as compared with CoCosNet [87] and CoCosNet v2 [93]. We also study the correspondence resolution (32×32 , 64×64 , 128×128), top- k number ($k=1, 2, 3$) and block size ($b=4, 16, 64$) in RAS. As Fig. 7 shows, the accuracy of the built correspondences keeps improving and the memory cost keeps increasing when image resolution or the top- k selection increases and the block size decreases. Compared with CoCosNet and CoCosNet v2, RAS reduces memory more clearly with the increase of correspondence resolution. With a trade-off between correspondence accuracy and memory cost, we select $k=3, b=4$ and correspondence resolution of 128×128 as the default setting of RAS.

In addition, we perform several ablation studies to examine the contribution of each loss by removing it from the overall objective. Table 8 show experimental results on the image translation task over ADE20K. As shown in Table 8, all involved losses contribute to the image translation in different manners and significance. Specially, the image quality as indicated by FID drops clearly without the perceptual loss \mathcal{L}_{perc} , and the style consistency as indicated by VGG_v decreases significantly with the removal of contextual loss \mathcal{L}_{ext} .

TABLE 6

Ablation studies on image translation and image manipulation tasks (both on ADE20K [91]): COS refer to Cosine similarity for building correspondence. RAS and CONFI denote the proposed ranking and attention scheme for building correspondence and confidence feature injection module in the generation network, respectively. PE and SPE refer to vanilla position encoding and the proposed semantic position encoding, respectively. Model in the last row is the standard RABIT.

Models	Image Translation					Image Manipulation				
	FID \downarrow	SWD \downarrow	LPIPS \uparrow	VGG ₅₂ \uparrow	VGG _V \uparrow	FID \downarrow	SWD \downarrow	PSNR \uparrow	VGG ₅₂ \uparrow	VGG _V \uparrow
SPADE	33.90	19.70	0.344	0.772	0.884	120.2	41.62	13.11	0.766	0.876
SPADE+COS	27.72	14.98	0.556	0.787	0.941	42.02	23.23	19.92	0.772	0.926
CONFI+COS	26.58	12.33	0.529	0.801	0.958	40.56	22.87	20.73	0.782	0.959
CONFI+RAS	25.51	11.94	0.548	0.807	0.966	33.32	18.89	21.97	0.785	0.964
CONFI+RAS+PE	24.93	10.20	0.578	0.791	0.974	28.32	16.48	22.79	0.797	0.971
CONFI+RAS+SPE*	24.35	9.893	0.596	0.812	0.977	26.61	15.05	23.08	0.802	0.975

TABLE 7

Ablation study of correspondence accuracy and memory cost with different correspondence size (32×32 , 64×64 , and 128×128), block size ($b=4$, 16, and 64) and top- k selection ($k=1$, 2, and 3) on DeepFashion [41] for image translation. The correspondence accuracy is evaluated by comparing the warped images and the ground truth with evaluation metrics L1, SSIM and PSNR. MC denotes the memory cost in gigabyte (GB). ** denotes the default setting of RAS.

Models	32 \times 32				64 \times 64				128 \times 128*			
	FID \downarrow	LPIPS \downarrow	SSIM \uparrow	MC \downarrow	FID \downarrow	LPIPS \downarrow	SSIM \uparrow	MC \downarrow	FID \downarrow	LPIPS \downarrow	SSIM \uparrow	MC \downarrow
CoCosNet [87]	102.9	0.402	0.621	6.179	64.43	0.298	0.630	11.23	54.87	0.273	0.657	21.73
CoCosNet v2 [93]	132.3	0.458	0.614	5.101	73.14	0.339	0.625	9.065	58.66	0.283	0.641	14.94
RAS ($k=1$, $b=64$)	144.1	0.470	0.608	4.912	97.79	0.367	0.618	8.986	76.47	0.333	0.622	14.35
RAS ($k=1$, $b=16$)	129.8	0.431	0.615	4.963	81.07	0.344	0.622	9.012	66.22	0.306	0.625	15.16
RAS ($k=1$, $b=4$)	102.4	0.382	0.620	5.093	70.12	0.321	0.624	9.082	59.97	0.292	0.634	15.95
RAS ($k=2$, $b=4$)	97.82	0.379	0.619	5.126	65.39	0.312	0.624	9.114	57.54	0.281	0.638	16.06
RAS ($k=3$, $b=4$)*	95.93	0.357	0.623	5.157	63.84	0.302	0.628	9.136	54.15	0.268	0.644	16.35

TABLE 8

Ablation studies of loss functions over ADE20K [91]. \mathcal{L}_{cyc} and \mathcal{L}_{cst} denote the cycle-consistency loss and feature consistency loss in the alignment network. \mathcal{L}_{per} , \mathcal{L}_{cxt} and \mathcal{L}_{pse} denote perceptual loss, contextual loss and pseudo pairs loss in the generation network.

Models	FID \downarrow	VGG ₅₂ \uparrow	VGG _V \uparrow
w/o \mathcal{L}_{cyc}	28.17	0.794	0.958
w/o \mathcal{L}_{cst}	29.27	0.809	0.962
w/o \mathcal{L}_{per}	45.16	0.738	0.861
w/o \mathcal{L}_{cxt}	35.05	0.798	0.853
w/o \mathcal{L}_{pse}	25.43	0.807	0.972
\mathcal{L}_{full}	24.35	0.812	0.977

5 CONCLUSIONS

This paper presents RABIT, a versatile conditional image translation & manipulation framework that adopts a novel bi-level alignment strategy with a ranking and attention scheme (RAS) to align the features between conditional inputs and exemplars efficiently. As the ranking operation precludes the gradient propagation in model training, we approximate it with a regularized earth mover's formulation which enables differentiable optimization of the ranking operation. A semantic position encoding mechanism is designed to facilitate semantic-level position information and preserve the texture patterns in the exemplars. To handle the semantic mismatching between the conditional inputs and warped exemplars, a novel confidence feature injection module is proposed to achieve multi-channel feature fusion based on the match-

ing reliability of warped exemplars. Quantitative and qualitative experiments over multiple datasets show that RABIT is capable of achieving high-fidelity image translation and manipulation while preserving consistent semantics with the conditional input and faithful styles with the exemplar.

The current exemplar-based image translation still requires the conditional input and the exemplar to be semantically similar in building meaningful correspondences, and this constrains the generalization of this translation approach. A possible solution is to further relax the constraint of exemplar selection. In this work, we propose the confidence feature injection module to mitigate the semantic discrepancy between conditional inputs and exemplars by assigning higher weights to the conditional input when the exemplar features are misaligned. However, adjusting fusion weights only mitigates the misalignment and the misaligned features still tend to mislead the generation process more or less. Instead of adjusting the fusion weights, we could rectify the misaligned features directly based on a pre-built feature bank with well-aligned features. These related issues will be studied in our future research.

6 ACKNOWLEDGEMENT

This study is supported under the RIE2020 Industry Alignment Fund – Industry Collaboration Projects (IAF-ICP) Funding Initiative, as well as cash and in-kind contribution from the industry partner(s).

REFERENCES

- [1] C. Barnes, E. Shechtman, A. Finkelstein, and D. B. Goldman. Patchmatch: A randomized correspondence algorithm for structural image editing. *ACM Trans. Graph.*, 28(3):24, 2009.
- [2] H. Bristow, J. Valmadre, and S. Lucey. Dense semantic correspondence where every pixel is a classifier. In *Proceedings of the IEEE International Conference on Computer Vision*, pages 4024–4031, 2015.
- [3] Z. Chen, C. Wang, B. Yuan, and D. Tao. Puppetergan: Arbitrary portrait animation with semantic-aware appearance transformation. In *Proceedings of the IEEE/CVF Conference on Computer Vision and Pattern Recognition*, pages 13518–13527, 2020.
- [4] Y. Choi, M. Choi, M. Kim, J.-W. Ha, S. Kim, and J. Choo. Stargan: Unified generative adversarial networks for multi-domain image-to-image translation. In *Proceedings of the IEEE Conference on Computer Vision and Pattern Recognition*, pages 8789–8797, 2018.
- [5] Y. Choi, Y. Uh, J. Yoo, and J.-W. Ha. Stargan v2: Diverse image synthesis for multiple domains. In *Proceedings of the IEEE/CVF Conference on Computer Vision and Pattern Recognition*, pages 8188–8197, 2020.
- [6] C. B. Choy, J. Gwak, S. Savarese, and M. Chandraker. Universal correspondence network. *arXiv preprint arXiv:1606.03558*, 2016.
- [7] K. Cui, G. Zhang, F. Zhan, and S. Lu. Fbc-gan: Diverse and flexible image synthesis via foreground-background composition. *arXiv preprint*, 2021.
- [8] M. Cuturi. Sinkhorn distances: Lightspeed computation of optimal transport. In *Advances in neural information processing systems*, pages 2292–2300, 2013.
- [9] Y. Dai, F. Gieseke, S. Oehmcke, Y. Wu, and K. Barnard. Attentional feature fusion. In *Proceedings of the IEEE/CVF Winter Conference on Applications of Computer Vision*, pages 3560–3569, 2021.
- [10] C. Doersch. Tutorial on variational autoencoders. *arXiv preprint arXiv:1606.05908*, 2016.
- [11] H. Dong, X. Liang, K. Gong, H. Lai, J. Zhu, and J. Yin. Soft-gated warping-gan for pose-guided person image synthesis. *arXiv preprint arXiv:1810.11610*, 2018.
- [12] Y. Fu, J. Ma, L. Ma, and X. Guo. Edit: Exemplar-domain aware image-to-image translation. *arXiv preprint arXiv:1911.10520*, 2019.
- [13] L. A. Gatys, A. S. Ecker, and M. Bethge. Image style transfer using convolutional neural networks. In *Proceedings of the IEEE conference on computer vision and pattern recognition*, pages 2414–2423, 2016.
- [14] S. Gu, J. Bao, H. Yang, D. Chen, F. Wen, and L. Yuan. Mask-guided portrait editing with conditional gans. In *Proceedings of the IEEE/CVF Conference on Computer Vision and Pattern Recognition*, pages 3436–3445, 2019.
- [15] B. Ham, M. Cho, C. Schmid, and J. Ponce. Proposal flow: Semantic correspondences from object proposals. *IEEE transactions on pattern analysis and machine intelligence*, 40(7):1711–1725, 2017.
- [16] K. Han, R. S. Rezende, B. Ham, K.-Y. K. Wong, M. Cho, C. Schmid, and J. Ponce. Scenet: Learning semantic correspondence. In *Proceedings of the IEEE international conference on computer vision*, pages 1831–1840, 2017.
- [17] M. He, D. Chen, J. Liao, P. V. Sander, and L. Yuan. Deep exemplar-based colorization. *ACM Transactions on Graphics (TOG)*, 37(4):1–16, 2018.
- [18] M. Heusel, H. Ramsauer, T. Unterthiner, B. Nessler, and S. Hochreiter. Gans trained by a two time-scale update rule converge to a local nash equilibrium. In *Advances in neural information processing systems*, pages 6626–6637, 2017.
- [19] J. Hoffman, E. Tzeng, T. Park, J.-Y. Zhu, P. Isola, K. Saenko, A. Efros, and T. Darrell. Cycada: Cycle-consistent adversarial domain adaptation. In *International conference on machine learning*, pages 1989–1998. PMLR, 2018.
- [20] S. Hong, X. Yan, T. Huang, and H. Lee. Learning hierarchical semantic image manipulation through structured representations. In *NIPS*, 2018.
- [21] A. Hosni, C. Rhemann, M. Bleyer, C. Rother, and M. Gelautz. Fast cost-volume filtering for visual correspondence and beyond. *IEEE Transactions on Pattern Analysis and Machine Intelligence*, 35(2):504–511, 2012.
- [22] X. Huang and S. Belongie. Arbitrary style transfer in real-time with adaptive instance normalization. In *Proceedings of the IEEE International Conference on Computer Vision*, pages 1501–1510, 2017.
- [23] X. Huang, M.-Y. Liu, S. Belongie, and J. Kautz. Multimodal unsupervised image-to-image translation. In *Proceedings of the European Conference on Computer Vision (ECCV)*, pages 172–189, 2018.
- [24] J. Hur, H. Lim, C. Park, and S. Chul Ahn. Generalized deformable spatial pyramid: Geometry-preserving dense correspondence estimation. In *Proceedings of the IEEE Conference on Computer Vision and Pattern Recognition*, pages 1392–1400, 2015.
- [25] P. Isola, J.-Y. Zhu, T. Zhou, and A. A. Efros. Image-to-image translation with conditional adversarial networks. In *Proceedings of the IEEE conference on computer vision and pattern recognition*, pages 1125–1134, 2017.
- [26] J. Johnson, A. Alahi, and L. Fei-Fei. Perceptual losses for real-time style transfer and super-resolution. In *European conference on computer vision*, pages 694–711. Springer, 2016.
- [27] L. V. Kantorovich. Mathematical methods of organizing and planning production. *Management science*, 6(4):366–422, 1960.
- [28] T. Karras, T. Aila, S. Laine, and J. Lehtinen. Progressive growing of gans for improved quality, stability, and variation. *arXiv preprint arXiv:1710.10196*, 2017.
- [29] J. Kim, C. Liu, F. Sha, and K. Grauman. Deformable spatial pyramid matching for fast dense correspondences. In *Proceedings of the IEEE Conference on Computer Vision and Pattern Recognition*, pages 2307–2314, 2013.
- [30] D. P. Kingma and M. Welling. Auto-encoding variational bayes. *arXiv preprint arXiv:1312.6114*, 2013.
- [31] W.-S. Lai, J.-B. Huang, N. Ahuja, and M.-H. Yang. Deep laplacian pyramid networks for fast and accurate super-resolution. In *Proceedings of the IEEE conference on computer vision and pattern recognition*, pages 624–632, 2017.
- [32] C. Ledig, L. Theis, F. Huszár, J. Caballero, A. Cunningham, A. Acosta, A. Aitken, A. Tejani, J. Totz, Z. Wang, et al. Photo-realistic single image super-resolution using a generative adversarial network. In *Proceedings of the IEEE conference on computer vision and pattern recognition*, pages 4681–4690, 2017.
- [33] C.-H. Lee, Z. Liu, L. Wu, and P. Luo. Maskgan: Towards diverse and interactive facial image manipulation. In *CVPR*, pages 5549–5558, 2020.
- [34] C.-H. Lee, Z. Liu, L. Wu, and P. Luo. Maskgan: Towards diverse and interactive facial image manipulation. In *IEEE Conference on Computer Vision and Pattern Recognition (CVPR)*, 2020.
- [35] Y. Li, Y. Cheng, Z. Gan, L. Yu, L. Wang, and J. Liu. Bachgan: High-resolution image synthesis from salient object layout. In *Proceedings of the IEEE Conference on Computer Vision and Pattern Recognition*, 2020.
- [36] Y. Li, C. Fang, J. Yang, Z. Wang, X. Lu, and M.-H. Yang. Universal style transfer via feature transforms. *arXiv preprint arXiv:1705.08086*, 2017.
- [37] J. Liao, Y. Yao, L. Yuan, G. Hua, and S. B. Kang. Visual attribute transfer through deep image analogy. *arXiv preprint arXiv:1705.01088*, 2017.
- [38] B. Lim, S. Son, H. Kim, S. Nah, and K. Mu Lee. Enhanced deep residual networks for single image super-resolution. In *Proceedings of the IEEE conference on computer vision and pattern recognition workshops*, pages 136–144, 2017.
- [39] H. Liu, B. Jiang, Y. Song, W. Huang, and C. Yang. Rethinking image inpainting via a mutual encoder-decoder with feature equalizations. In *ECCV*, pages 725–741, 2020.
- [40] R. Liu, J. Lehman, P. Molino, F. Petroski Such, E. Frank, A. Sergeev, and J. Yosinski. An intriguing failing of convolutional neural networks and the coordconv solution. In *Advances in Neural Information Processing Systems*, 2018.
- [41] Z. Liu, P. Luo, S. Qiu, X. Wang, and X. Tang. Deepfashion: Powering robust clothes recognition and retrieval with rich annotations. In *Proceedings of the IEEE conference on computer vision and pattern recognition*, pages 1096–1104, 2016.
- [42] Z. Liu, P. Luo, X. Wang, and X. Tang. Deep learning face attributes in the wild. In *Proceedings of the IEEE international conference on computer vision*, pages 3730–3738, 2015.
- [43] J. Long, N. Zhang, and T. Darrell. Do convnets learn correspondence? *arXiv preprint arXiv:1411.1091*, 2014.
- [44] D. G. Lowe. Distinctive image features from scale-invariant keypoints. *International journal of computer vision*, 60(2):91–110, 2004.
- [45] J. Lucas, G. Tucker, R. Grosse, and M. Norouzi. Don’t blame the elbo! a linear vae perspective on posterior collapse. *arXiv preprint arXiv:1911.02469*, 2019.
- [46] G. Luise, A. Rudi, M. Pontil, and C. Ciliberto. Differential properties of sinkhorn approximation for learning with wasserstein distance. In *NIPS 2018-Advances in Neural Information Processing Systems*, pages 5864–5874, 2018.
- [47] L. Ma, X. Jia, S. Georgoulis, T. Tuytelaars, and L. Van Gool. Exemplar guided unsupervised image-to-image translation with semantic consistency. In *International Conference on Learning Representations*, 2018.
- [48] L. Ma, X. Jia, Q. Sun, B. Schiele, T. Tuytelaars, and L. Van Gool. Pose guided person image generation. In *Advances in neural information processing systems*, pages 406–416, 2017.
- [49] R. Mechrez, I. Talmi, and L. Zelnik-Manor. The contextual loss for image transformation with non-aligned data. In *Proceedings of the European Conference on Computer Vision (ECCV)*, pages 768–783, 2018.
- [50] Y. Men, Y. Mao, Y. Jiang, W.-Y. Ma, and Z. Lian. Controllable person image synthesis with attribute-decomposed gan. In *Proceedings of the IEEE/CVF Conference on Computer Vision and Pattern Recognition*, pages 5084–5093, 2020.
- [51] Z. Murez, S. Kolouri, D. Kriegman, R. Ramamoorthi, and K. Kim. Image to image translation for domain adaptation. In *Proceedings of the IEEE conference on computer vision and pattern recognition*, pages 1125–1134, 2017.

Conference on Computer Vision and Pattern Recognition, pages 4500–4509, 2018.

[52] E. Ntavellas, A. Romero, I. Kastanis, L. Van Gool, and R. Timofte. Sesame: Semantic editing of scenes by adding, manipulating or erasing objects. In *ECCV*, pages 394–411. Springer, 2020.

[53] M. Okutomi and T. Kanade. A multiple-baseline stereo. *IEEE Transactions on pattern analysis and machine intelligence*, 15(4):353–363, 1993.

[54] T. Park, M.-Y. Liu, T.-C. Wang, and J.-Y. Zhu. Semantic image synthesis with spatially-adaptive normalization. In *Proceedings of the IEEE Conference on Computer Vision and Pattern Recognition*, pages 2337–2346, 2019.

[55] A. Pumarola, A. Agudo, A. M. Martinez, A. Sanfeliu, and F. Moreno-Noguer. Ganimation: Anatomically-aware facial animation from a single image. In *Proceedings of the European Conference on Computer Vision (ECCV)*, pages 818–833, 2018.

[56] A. Shrivastava, T. Pfister, O. Tuzel, J. Susskind, W. Wang, and R. Webb. Learning from simulated and unsupervised images through adversarial training. In *Proceedings of the IEEE conference on computer vision and pattern recognition*, pages 2107–2116, 2017.

[57] A. Shrivastava, T. Pfister, O. Tuzel, J. Susskind, W. Wang, and R. Webb. Learning from simulated and unsupervised images through adversarial training. In *Proceedings of the IEEE conference on computer vision and pattern recognition*, pages 2107–2116, 2017.

[58] K. Simonyan and A. Zisserman. Very deep convolutional networks for large-scale image recognition. *arXiv preprint arXiv:1409.1556*, 2014.

[59] W. Sun and T. Wu. Image synthesis from reconfigurable layout and style. In *Proceedings of the IEEE International Conference on Computer Vision*, pages 10531–10540, 2019.

[60] H. Tang, D. Xu, G. Liu, W. Wang, N. Sebe, and Y. Yan. Cycle in cycle generative adversarial networks for keypoint-guided image generation. In *Proceedings of the 27th ACM International Conference on Multimedia*, pages 2052–2060, 2019.

[61] H. Tang, D. Xu, N. Sebe, Y. Wang, J. J. Corso, and Y. Yan. Multi-channel attention selection gan with cascaded semantic guidance for cross-view image translation. In *Proceedings of the IEEE Conference on Computer Vision and Pattern Recognition*, pages 2417–2426, 2019.

[62] Y.-H. Tsai, W.-C. Hung, S. Schulter, K. Sohn, M.-H. Yang, and M. Chandraker. Learning to adapt structured output space for semantic segmentation. In *Proceedings of the IEEE conference on computer vision and pattern recognition*, pages 7472–7481, 2018.

[63] Z. Wan, B. Zhang, D. Chen, P. Zhang, D. Chen, J. Liao, and F. Wen. Bringing old photos back to life. In *Proceedings of the IEEE/CVF Conference on Computer Vision and Pattern Recognition*, pages 2747–2757, 2020.

[64] M. Wang, G.-Y. Yang, R. Li, R.-Z. Liang, S.-H. Zhang, P. M. Hall, and S.-M. Hu. Example-guided style-consistent image synthesis from semantic labeling. In *Proceedings of the IEEE/CVF Conference on Computer Vision and Pattern Recognition*, pages 1495–1504, 2019.

[65] T.-C. Wang, M.-Y. Liu, J.-Y. Zhu, A. Tao, J. Kautz, and B. Catanzaro. High-resolution image synthesis and semantic manipulation with conditional gans. In *Proceedings of the IEEE conference on computer vision and pattern recognition*, pages 8798–8807, 2018.

[66] Y. Wang, X. Tao, X. Qi, X. Shen, and J. Jia. Image inpainting via generative multi-column convolutional neural networks. In *Advances in Neural Information Processing Systems*, pages 331–340, 2018.

[67] R. Wu and S. Lu. Leed: Label-free expression editing via disentanglement. In *European Conference on Computer Vision*, pages 781–798. Springer, 2020.

[68] R. Wu, G. Zhang, S. Lu, and T. Chen. Cascade ef-gan: Progressive facial expression editing with local focuses. In *Proceedings of the IEEE/CVF Conference on Computer Vision and Pattern Recognition*, pages 5021–5030, 2020.

[69] W. Xia, Y. Yang, J.-H. Xue, and B. Wu. Tedigan: Text-guided diverse face image generation and manipulation. In *Proceedings of the IEEE/CVF Conference on Computer Vision and Pattern Recognition*, pages 2256–2265, 2021.

[70] Y. Xie, H. Dai, M. Chen, B. Dai, T. Zhao, H. Zha, W. Wei, and T. Pfister. Differentiable top-k with optimal transport. *Advances in Neural Information Processing Systems*, 33, 2020.

[71] J. Yu, Z. Lin, J. Yang, X. Shen, X. Lu, and T. S. Huang. Free-form image inpainting with gated convolution. In *ICCV*, pages 4471–4480, 2019.

[72] Y. Yu, F. Zhan, R. Wu, J. Pan, K. Cui, S. Lu, F. Ma, X. Xie, and C. Miao. Diverse image inpainting with bidirectional and autoregressive transformers. *arXiv preprint arXiv:2104.12335*, 2021.

[73] F. Zhan and S. Lu. Esir: End-to-end scene text recognition via iterative image rectification. In *Proceedings of the IEEE Conference on Computer Vision and Pattern Recognition*, pages 2059–2068, 2019.

[74] F. Zhan, S. Lu, and C. Xue. Verisimilar image synthesis for accurate detection and recognition of texts in scenes. In *Proceedings of the European Conference on Computer Vision (ECCV)*, pages 249–266, 2018.

[75] F. Zhan, S. Lu, C. Zhang, F. Ma, and X. Xie. Adversarial image composition with auxiliary illumination. In *Proceedings of the Asian Conference on Computer Vision*, 2020.

[76] F. Zhan, S. Lu, C. Zhang, F. Ma, and X. Xie. Towards realistic 3d embedding via view alignment. *arXiv preprint arXiv:2007.07066*, 2020.

[77] F. Zhan, C. Xue, and S. Lu. Ga-dan: Geometry-aware domain adaptation network for scene text detection and recognition. In *Proceedings of the IEEE International Conference on Computer Vision*, pages 9105–9115, 2019.

[78] F. Zhan, Y. Yu, K. Cui, G. Zhang, S. Lu, J. Pan, C. Zhang, F. Ma, X. Xie, and C. Miao. Unbalanced feature transport for exemplar-based image translation. In *Proceedings of the IEEE Conference on Computer Vision and Pattern Recognition*, 2021.

[79] F. Zhan, Y. Yu, R. Wu, C. Zhang, S. Lu, L. Shao, F. Ma, and X. Xie. Gmlight: Lighting estimation via geometric distribution approximation. *arXiv preprint arXiv:2102.10244*, 2021.

[80] F. Zhan and C. Zhang. Spatial-aware gan for unsupervised person re-identification. In *2020 25th International Conference on Pattern Recognition (ICPR)*, pages 6889–6896. IEEE, 2021.

[81] F. Zhan, C. Zhang, W. Hu, S. Lu, F. Ma, X. Xie, and L. Shao. Sparse needlets for lighting estimation with spherical transport loss. *arXiv preprint arXiv:2106.13090*, 2021.

[82] F. Zhan, C. Zhang, Y. Yu, Y. Chang, S. Lu, F. Ma, and X. Xie. Emlight: Lighting estimation via spherical distribution approximation. *arXiv preprint arXiv:2012.11116*, 2020.

[83] F. Zhan, H. Zhu, and S. Lu. Scene text synthesis for efficient and effective deep network training. *arXiv preprint arXiv:1901.09193*, 2019.

[84] F. Zhan, H. Zhu, and S. Lu. Spatial fusion gan for image synthesis. In *Proceedings of the IEEE conference on computer vision and pattern recognition*, pages 3653–3662, 2019.

[85] B. Zhang, M. He, J. Liao, P. V. Sander, L. Yuan, A. Bermak, and D. Chen. Deep exemplar-based video colorization. In *Proceedings of the IEEE Conference on Computer Vision and Pattern Recognition*, pages 8052–8061, 2019.

[86] J. Zhang, S. Lu, F. Zhan, and Y. Yu. Blind image super-resolution via contrastive representation learning. *arXiv preprint arXiv:2107.00708*, 2021.

[87] P. Zhang, B. Zhang, D. Chen, L. Yuan, and F. Wen. Cross-domain correspondence learning for exemplar-based image translation. In *Proceedings of the IEEE/CVF Conference on Computer Vision and Pattern Recognition*, pages 5143–5153, 2020.

[88] R. Zhang, P. Isola, A. A. Efros, E. Shechtman, and O. Wang. The unreasonable effectiveness of deep features as a perceptual metric. In *Proceedings of the IEEE conference on computer vision and pattern recognition*, pages 586–595, 2018.

[89] B. Zhao, L. Meng, W. Yin, and L. Sigal. Image generation from layout. In *Proceedings of the IEEE Conference on Computer Vision and Pattern Recognition*, pages 8584–8593, 2019.

[90] H. Zheng, Z. Lin, J. Lu, S. Cohen, J. Zhang, N. Xu, and J. Luo. Semantic layout manipulation with high-resolution sparse attention. *arXiv preprint arXiv:2012.07288*, 2020.

[91] B. Zhou, H. Zhao, X. Puig, S. Fidler, A. Barriuso, and A. Torralba. Scene parsing through ade20k dataset. In *Proceedings of the IEEE conference on computer vision and pattern recognition*, pages 633–641, 2017.

[92] T. Zhou, P. Krahenbuhl, M. Aubry, Q. Huang, and A. A. Efros. Learning dense correspondence via 3d-guided cycle consistency. In *Proceedings of the IEEE Conference on Computer Vision and Pattern Recognition*, pages 117–126, 2016.

[93] X. Zhou, B. Zhang, T. Zhang, P. Zhang, J. Bao, D. Chen, Z. Zhang, and F. Wen. Cocosnet v2: Full-resolution correspondence learning for image translation. In *CVPR*, 2021.

[94] J.-Y. Zhu, P. Krähenbühl, E. Shechtman, and A. A. Efros. Generative visual manipulation on the natural image manifold. In *ECCV*, pages 597–613. Springer, 2016.

[95] P. Zhu, R. Abdal, Y. Qin, and P. Wonka. Sean: Image synthesis with semantic region-adaptive normalization. In *Proceedings of the IEEE/CVF Conference on Computer Vision and Pattern Recognition*, pages 5104–5113, 2020.

[96] Z. Zhu, Z. Xu, A. You, and X. Bai. Semantically multi-modal image synthesis. In *Proceedings of the IEEE/CVF Conference on Computer Vision and Pattern Recognition*, pages 5467–5476, 2020.

Fangneng Zhan received the B.E. degree in Communication Engineering and Ph.D. degree in Computer Science & Engineering from the University of Electronic Science and Technology of China and Nanyang Technological University, respectively. He will join the Inception Institute of Artificial Intelligence (IIAI) as a research associate. His research interests include deep generative models, image synthesis and manipulation. He contributed to the research field by publishing more than

10 articles in prestigious conferences. He also served as a reviewer or program committee member for top conferences including ICLR, NeurIPS, CVPR, ICCV, ECCV, AAAI.

Yingchen Yu obtained the B.E. degree in Electrical & Electronic Engineering at Nanyang Technological University, and M.S. degree in Computer Science at National University of Singapore. He is currently pursuing the Ph.D. degree at School of Computer Science and Engineering, Nanyang Technological University under Alibaba Talent Programme. His research interests include computer vision and machine learning, specifically for image synthesis and manipulation.

Rongliang Wu received the B.E. degree in Information Engineering from South China University of Technology, and M.S. degree in Electrical and Computer Engineering from National University of Singapore. He is currently pursuing the Ph.D. degree at School of Computer Science and Engineering, Nanyang Technological University. His research interests include computer vision and deep learning, specifically for facial expression analysis and generation.

Kaiwen Cui obtained the B.E. degree in Electrical Engineering at National University of Singapore, and M.S. degree in Electrical Engineering at National University of Singapore. He is currently pursuing the Ph.D. degree at School of Computer Science and Engineering, Nanyang Technological University. His research interests include computer vision and machine learning, specifically for image synthesis.

Aoran Xiao received the BS and MS degrees from Wuhan University in 2016 and 2019. He is currently pursuing the PhD degree at School of Computer Science and Engineering, Nanyang Technological University. His research interests include deep learning, point cloud processing and computer vision.

Shijian Lu is an Assistant Professor in the School of Computer Science and Engineering, Nanyang Technological University. He received his PhD in Electrical and Computer Engineering from the National University of Singapore. His research interests include computer vision and deep learning. He has published more than 100 internationally refereed journal and conference papers. Dr Lu is currently an Associate Editor for the journals of Pattern Recognition and Neurocomputing.

Ling Shao is the CEO and the Chief Scientist of the Inception Institute of Artificial Intelligence (IIAI), Abu Dhabi, United Arab Emirates. He was also the initiator and the Founding Provost and Executive Vice President of the Mohamed bin Zayed University of Artificial Intelligence (the world's first AI University), UAE. His research interests include computer vision, deep learning, medical imaging and vision and language. He is a fellow of the IEEE, the IAPR, the IET, and the BCS.